ISSN 1063-7834, Physics of the Solid State, 2011, Vol. 53, No. 12, pp. 2435–2440. © Pleiades Publishing, Ltd., 2011.
Original Russian Text © S.V. Melnikova, A.D. Vasilev, A.G. Kocharova, 2011, published in Fizika Tverdogo Tela, 2011, Vol. 53, No. 12, pp. 2312–2317.

DIELECTRICS

The Role of Structural and Nonstructural Water in Oxyfluoride $K_2WO_2F_4 \cdot H_2O$

S. V. Melnikova*, A. D. Vasilev, and A. G. Kocharova

Kirensky Institute of Physics, Siberian Branch of the Russian Academy of Sciences, Akademgorodok 50, Krasnoyarsk, 660036 Russia

** e-mail: msv@iph.krasn.ru*

Received May 24, 2011

Abstract—X-ray structural and polarization optical investigations have been performed, and birefringence and rotation angles of the optical indicatrix φ_b and φ_c of the $K_2WO_2F_4 \cdot H_2O$ crystal have been measured in the temperature range of 100–600 K. The structure and symmetry of compounds at room temperature have been refined. It has been established that the layered crystal $K_2WO_2F_4 \cdot H_2O$ can exist in two states (A and B) depending on the atmospheric humidity and undergoes the sequence of reversible and irreversible phase transformations $G_3 \longleftrightarrow G_2 \longrightarrow G_1 \longrightarrow G_0$. The sequences of changes in the phase symmetry $P\bar{1} \longleftrightarrow C2/m \longrightarrow P4/nmm$ for samples A and $m \longleftrightarrow C2/m \longrightarrow P4/nmm$ for samples B have been found. The second-order proper ferroelastic phase transition ($P\bar{1} \longleftrightarrow C2/m$) at $T_{03} = 270$–290 K ($G_3 \longleftrightarrow G_2$) is accompanied by twinning and appearance of the shift deformation x_6. The crystal system of the substance for the B crystals remains invariable after the second-order phase transition $G_3 \longleftrightarrow G_2$. The irreversible first-order phase transition $G_2 \longrightarrow G_1$ occurs in a temperature range $T_{02} \approx 350$–380 K; it is accompanied by the loss of the crystallization water, which then is reduced easily from the atmosphere for a day. The substance decomposes at $T_{01} \approx 510$ K ($G_1 \longrightarrow G_0$). The distinction between the A and B crystals has been explained by the presence or absence of free water in interlayer spacings.

DOI: 10.1134/S1063783411120146

1. INTRODUCTION

Oxyfluoride compounds with the general formula A_2BX_6 (where A = K, Rb, Cs, Na, NH_4; B = Nb, Mo, W; and X = O(F)) have been actively studied with various physical methods for several years [1–15]. These crystals are of interest owing to the possibility to obtain new functional acentrosymmetric materials with a broad transparency range because the structure of these substances consists of cations A and isolated polar oxyfluoride complexes $[BX_6]^{2-}$. Depending on the size and shape of cations $[A]^+$, the structures of both various symmetry (trigonal [1, 4], tetragonal [5, 6], and orthorhombic [2–4, 8]) and with various degrees of ordering of quasi-octahedron complexes are formed in the family. The positive result in the search for acentrosymmetric crystals is attained for substances with an organic $[A]^+$ cation [7, 8]. There is no information on the phase transitions in compounds with atomic cations. The possibility of structural transformation $P4/nmm \longrightarrow P4/n$ caused by ordering of the $[NbOF_5]^{2-}$ complex is assumed only for K_2NbOF_5 [6]. The substitution of the atomic cation by ammonium one promotes the additional disordering in oxyfluorides and increases the probability of structural transformations in them [9–11].

A comparative analysis of the properties and structure of the substances with the formula A_2BX_6 showed the feature of potassium-containing crystals [5, 6, 12–15]. The anion groups BX_6 in these substances are isolated and arranged so that they form two types of interoctahedral polyhedra. The half of potassium ions is arranged in octahedral voids formed by the vertices of six neighboring complexes BX_6. Other potassium atoms occupy only half of twelve-coordinated polyhedra formed by the faces of BX_6 groups. Free voids can be filled with water. For this reason, crystals with potassium possess well hygroscopic properties, while upon growing from aqueous solutions, crystal hydrates are always formed. In this case, the general motif of the structure of hydrates and nonhydrates is retained, although certain distinction of atomic coordinates and unit cell parameters occurs. The crystal symmetry also differs. For example, unhydrous crystals $K_2MoO_2F_4$, K_2NbOF_5, and $K_2WO_2F_4$ have symmetry $P4/nmm$ [5, 6, 15], while crystal hydrates grow monoclinic with various space groups, namely, $K_2NbOF_5 \cdot H_2O$ and $K_2MoO_2F_4 \cdot H_2O$ have symmetry $P2_1/c$ ($a \approx 6.2$ Å, $b \approx 6.2$ Å, $c \approx 18.2$ Å, $\beta \approx 96°$, $Z = 4$) [12, 13], and $K_2MoO_2F_5 \cdot H_2O$ has symmetry $C2/m$ ($a \approx 8.5$ Å, $b \approx 8.5$ Å, $c \approx 9.1$ Å, $\beta \approx 100°$, $Z = 4$) [14]. Starting from similarity of X-ray diffraction patterns for the

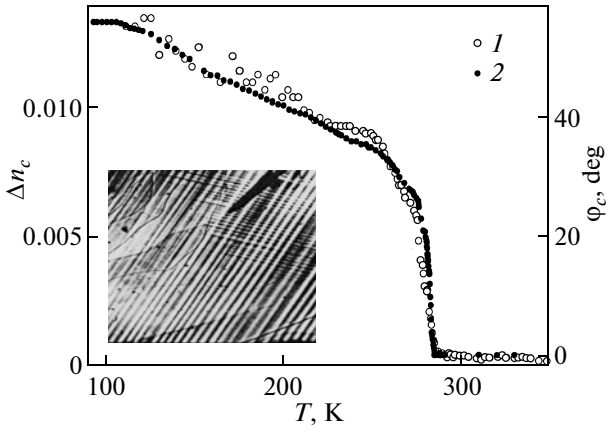

Fig. 1. Temperature dependences of (*1*) birefringence $\Delta n_c(T)$ and (*2*) tilting angle of the optical indicatrix $\varphi_c(T)$ in the $K_2WO_2F_4 \cdot H_2O$ crystal (sample A). The twin pattern of the phase G_3 in the (001) plate (sample A) is in inset.

$K_2WO_2F_4$ and $K_2WO_2F_4 \cdot H_2O$ crystals and similar molybdates [5, 13], authors of [15] selected the same symmetry groups for tungsten compounds. Namely, the $K_2WO_2F_4 \cdot H_2O$ crystal has symmetry $P2_1/c$ and unit cell parameters $a \approx 6.216$ Å, $b \approx 6.234$ Å, $c \approx 18.186$ Å, $\beta \approx 96.20°$, and $Z = 4$. Stability of water-containing oxyfluorides is unknown.

We synthesized and grew $K_2WO_2F_4 \cdot H_2O$ single crystals, performed polarization optical and X-ray investigations, and measurements of birefringence of the extinction angle in the temperature range 100–400 K in order to search and investigate the phase transitions and to determine the phase symmetry. The complex of performed investigations showed that depending on the storage conditions, the $K_2WO_2F_4 \cdot H_2O$ crystals can exist in states A and B. Samples A are the as-grown or placed into the medium with an increased humidity (from 20 to 100%) crystals, and samples B are the crystals that were stored more than year in a dry room (relative humidity less than 20%).

2. CRYSTAL GROWTH

The $K_2WO_2F_4$ compound was synthesized during mixing potassium tungstate and 40% hydrofluoric acid: $K_2WO_4 + 4HF = K_2WO_2F_4 + 2H_2O$. Crystallization was performed at 303 K during drying a white suspension formed after the reaction. Transparent $K_2WO_2F_4 \cdot H_2O$ crystals with various habits are obtained. These are mainly rectangular mica-like (001) plates with an ideal cleavage plane and "direct" extinctions as well as rhombohedral plates of the (010) cut with "indirect" extinctions. The habit and crystal–optical characteristics of obtained samples correspond to monoclinic symmetry, but the shape of the (010) growth plates indicates that the monoclinicity angle of this substance is of about 99°, while $\beta = 96.20°$ according to [15]. This fact initiated the X-ray structural studies of obtained crystals. The polarization–optical studies of the grown (001) and (010) single-crystal samples were performed using an Axioskop-40 microscope; the rotation angle of the optical indicatrix and birefringence were measured by the Berek method accurate to ±0.0001.

3. OPTICAL INVESTIGATIONS

The polarization–optical studies of $K_2WO_2F_4 \cdot H_2O$ at room temperature revealed no difference between the samples in states A and B. The difference manifests itself only in the temperature region below room temperature. In the plate of the cut (001) in state A near the melting point of ice, a bright twin pattern appears in a view field of the polarization microscope, in which the components differ by the extinction position for angle $2\varphi_c$ (Fig. 1). With the further cooling, the twins are expanded, and then one of the components disappears completely. The temperature, at which twins are formed in the crystal (T_{03}) considerable differs for various samples as $T_{03} = 270$–290 K. For the plate under study, $T_{03} = 285$ K. The temperature behavior of the rotation angle of the optical indicatrix $\varphi_c(T)$ in a separate twin is shown in Fig. 1 (points *2*). In the temperature region above $T = T_{03}$, tilting around [001] is absent, and the rotation angle at $T \le T_{03}$ initially varies slowly and then rapidly increases reaching extraordinary large magnitude $\varphi_c > 50°$.

In contrast with crystal A, the "direct extinction" in the (001) plate retains in state B in the temperature range 90–380 K. At $T \le 263$ K, we can observe a twin pattern constituting the shapeless spots differing only by the magnitude of birefringence (Fig. 2). Above $T'_{03} = 263$ K, the spots disappear. During heating, samples A and B become optically isotropic in a temperature range $T_{02} \approx 350$–380 K. At $T_{01} \approx 510$ K, the crystals destroy and become opaque.

The results of temperature measurements of birefringence $\Delta n_c(T)$ of crystals A are presented in Fig. 1 (points *1*). Because of the appearance of a large revolution angle $\varphi_c(T)$ in a low-temperature region, the sample was additionally oriented in each temperature point during measuring the birefringence $\Delta n_c(T)$ in order to superpose with the coordinate of the optical indicatrix. The superposition procedure of the coordinates decreases the accuracy of measuring the birefringence; therefore, the spread of the values of Δn_c is noticeable in Fig. 1. According to Fig. 1, the optical anisotropy in a high-temperature region is small and insignificantly changes from $\Delta n_c \approx 0.0003$ at 340 K to $\Delta n_c \approx 0.0004$ at 285 K. Birefringence starts to abruptly increase at $T < T_{03}$ and reaches the value $\Delta n_c \approx 0.0130$

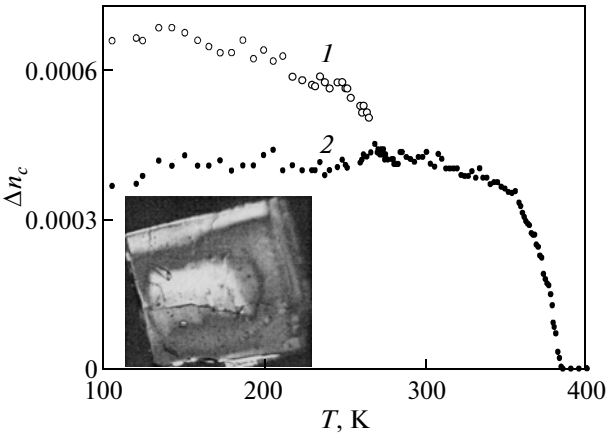

Fig. 2. Temperature dependence of birefringence $\Delta n_c(T)$ in the $K_2WO_2F_4 \cdot H_2O$ (sample B). Curves *1* and *2* correspond to birefringence in various twins. The form of the twins of phase G_3 in the (001) plate (sample B) is in inset.

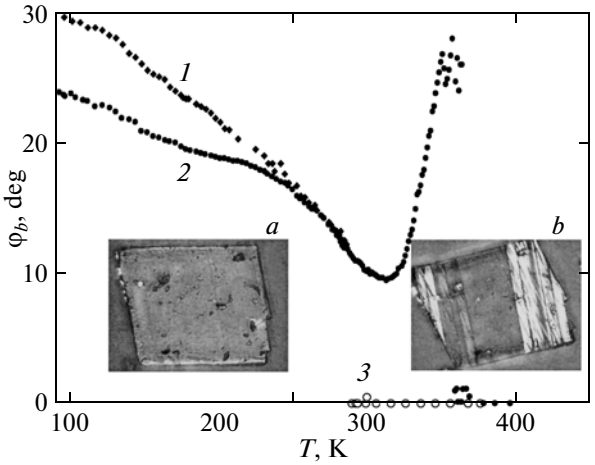

Fig. 3. Temperature behavior of the rotation angle of the optical indicatrix $\varphi_b(T)$ in the $K_2WO_2F_4 \cdot H_2O$ crystals. (*1*) Sample A, (*2*) sample B, and (*3*) sample B during cooling. The insets show (*a*) the shape of the (010) plate and (*b*) the initial stage of the phase transition $G_2 \longleftrightarrow G_1$.

at 100 K. It is seen that the dependences $\Delta n_c(T)$ and $\varphi_c(T)$ below T_{03} are similar (Fig. 1).

The temperature dependence of birefringence $\Delta n_c(T)$ of the $K_2WO_2F_4 \cdot H_2O$ crystal in state B is presented in Fig. 2. Curves *1* and *2* correspond to $\Delta n_c(T)$ in different twins. It is seen that the difference in the magnitude of birefringence for the spots (Fig. 2) is small and occurs only in the temperature range 90–263 K. The room-temperature optical anisotropy of the samples is the same. The difference of samples A and B manifests itself in the low-temperature region. Upon cooling, birefringence of crystals A abruptly increases as a result of the phase transition at $T_{03} =$ 285 K (Fig. 1), while the optical anisotropy of samples B changes weakly (Fig. 2). During heating the birefringence gradually decreases, and at $T = T_{02}$ we have $\Delta n_c = 0$. Cut (001) becomes isotropic. During cooling, this state is retained down to liquid-nitrogen temperature.

Rhomb-like samples of the growth of cut (010) can be monodomain or have the lamellar twin structure differing by the turns of indicatrices in neighboring region for the angle $2\varphi_b \approx 20°$. The temperature dependence of the extinction angle $\varphi_b(T)$ of such a plate has an unusual form (Fig. 3). Room-temperature $\varphi_b \approx 10°$ gradually increases during cooling to $\varphi_b \approx 30°$ in crystals A (curve *1*) and $\varphi_b \approx 24°$ in samples B (curve *2*). Such dependences $\varphi_b(T)$ in the low-temperature region imply a gradual decrease in angle φ_b to zero upon heating with the possible phase transition into the orthorhombic phase. However, the experiment showed that during heating with a low rate $dT/dt \approx 1$ K/min, $\varphi_b \approx 10°$ is retained in the temperature range 300–320 K and then gradually increases to $\varphi_b \approx 27°$ at 350 K (Fig. 3, curve *1*). Upon the further heating, the sample starts to crack along the cleavage plane (001), and headland bright strips gradually filling the entire sample volume appear in it (inset *b* in Fig. 3). Extinction in sample A becomes difficult to be determinable and nonuniform. This prolonged process is reversible at the first stage; during cooling, the clear extinction of the samples is retained. An increase in the heating rate leads to the shift of the region of increasing $\varphi_b(T)$ towards high temperatures. In crystals B, the regions with direct extinction are irreversibly formed in this temperature range; they gradually fill the whole volume of the sample. Above 380 K, angle $\varphi_b = 0$. During cooling, the direct extinction is retained (Fig. 3, curve *3*).

4. X-RAY INVESTIGATIONS

The structure of the $K_2WO_2F_4 \cdot H_2O$ in states A and B is studied using a SMART APEX II (Bruker AXS) single-crystal X-ray diffractometer with a CCD detector and MoK_α radiation for monodomain plates of the (001) cut at room temperature. The structure is determined by direct methods and refined in the anisotropic approximation of thermal atomic vibrations (SHELXTL [16]). The crystallographic data and the features of refinement are presented in the table.

The main structural units of this substance are isolated slightly distorted $WF(O)_6$ octahedra (Fig. 4a) with potassium ions and water molecules arranged in the voids between octahedra. The lattice contains two independent potassium ions (K1 and K2) and symmetrically independent molecule of the crystallized (structural) water.

Refinement showed that the fluorine and oxygen atoms compete in two sites; in both sites, the F/O ratio is 2/1. All atoms of the octahedron excluding F(O)2

Experimental data and refinement parameters of the structure of $K_2WO_2F_4 \cdot H_2O$

Parameter	Numerical value
Experimental data	
T, K*	298
Z	4
$2\theta_{max}$, deg	57
a, b, c, Å	8.791(1), 8.792(1), 9.152(1)
β, deg	98.675(1)
V, Å^3	699.2(1)
d, g/cm^3	3.668
μ, mm^{-1}	17.737
Number of measured reflections	3154
Number of independent reflections	942
Number of reflections with $F > 4\sigma_F$	923
Ranges of h, k, l	$-11 \le h \le 11$; $-11 \le K \le 11$; $-12 \le l \le 12$
Refinement results	
Weight refinement over F^2	$w = [\sigma^2(F_0^2) + (0.0431P)^2 + 0.5719P]^{-1}$, where $P = [\max(F_0^2, 0) + 2F_c^2]/3$
Number of refined parameters	63
$R1$ $[F_0 > 4\sigma(F_0)]$	0.0252
$wR2$	0.0685
Extinction parameter	0.0015(1)
GooF	1.07
$(\Delta\rho)_{max}$, e/Å^3	1.62
$(\Delta\rho)_{min}$, e/Å^3	−1.02
$(\Delta/\sigma)_{max}$	0

Note: GooF is the quality of refinement (Goodness of fit), F is the structural amplitude, F^2 is the structural factor, F_c denotes the calculated value, F_0 denotes the experimental value, and w is the weight coefficient.

are arranged on a mirror plane. The tungsten atom is shifted from the center to the O5 atom and most remote from F1 and F3 (distances are presented in Å): W–O5 = 1.738(6), W–F(O)4 = 1.844(5), W–F(O)2 = 1.883(4), W–F1 = 2.014(5), W–F3 = 1.938(4). The corresponding angles have the values from 81.7(2)° (F1–W–F3) to 97.4(1)° (F(O)4–W–O5). The K1 atom has tetrahedral surrounding consisting of tungsten atoms. Two pairs of water molecules are added to six $WF(O)_6$ octahedra; when substituting the water molecules by average sites $(Ow)_m$, we acquired the following K1–W distances: 2 × 4.449, 4.401, 4.496, 4.412, and 4.884(3) Å. Six bonds K1–F(O) and two K1–$(Ow)_m$ form the pattern presented in Fig. 4b. The distances in the bonds are (in Å): K1–F(O)2 = 2.699(4), K1–$(Ow)_m$ = 2.87(4), K1–F(O)4 = 2.716(4), K1–F1 = 2.876(4), K1–F3 = 2.657(4), and K1–O5 = 2.767(4). The K2 atom is tetrahedrically surrounded by tungsten atoms: 2 × 3.768(3), 2 × 3.732(3) Å, and W–K–W angles have the values in the range from 108° to 112°. Four faces of octahedra, which form the surrounding shaped as a distorted cub-octahedron, are nearest to K2, and distances K2–F(O) enter the range from 2.831(4) to 3.191(4) Å.

Water molecules occupy the disordered location around the second-order axis. They are coordinated by octahedra so that the middles of their edges tetrahedrically surround O_w. Distances $(Ow)_m$–F(O) are 2 × 3.18(4), 2 × 3.19(4), 2 × 3.35(4), and 2 × 3.44(4) Å. We failed to find locations of hydrogen atoms in water molecules; however, judging by distances, we can assume the existence of hydrogen bonds between water molecules and all ligands.

X-ray studies of single-crystal $K_2WO_2F_4 \cdot H_2O$ samples at room temperature showed the complete coincidence of the structure and symmetry of this substance in states A and B with identical population with the molecules of crystallization water.

5. RESULTS AND DISCUSSION

Our X-ray investigations of the $K_2WO_2F_4 \cdot H_2O$ compound allowed us to determine the structure and symmetry of this substance at room temperature. Although the general motif of the structure repeats for potassium-containing compounds [5, 6, 12–15], results of our investigations are different [13, 15]. First, it is established that the $K_2WO_2F_4 \cdot H_2O$ compound has the symmetry group $C2/m$ at room temperature rather than $P2_1/c$ [15]. This fact agrees with the crystal habit (inset *a* in Fig. 3), where β ≈ 99°. It is noteworthy that the symmetry and unit cell parameters of the crystal lattice for $K_2WO_2F_4 \cdot H_2O$ (the table) are very close to the data acquired for the $K_2WO_2F_5 \cdot H_2O$ crystal [14]. Second, we succeeded to establish the presence of the competitive arrangement of oxygen and fluorine atoms in two octahedron sites with the F/O ratio of 2/1 (Fig. 4a), while according to [13], both oxygen atoms occupy the sites on a mirror plane. Third, the experimental data allowed us to select the model of the structure with disordering of the crystallized water in two sites around the second-order axis. This fact indicates the possibility of lowering the symmetry of the crystal hydrate upon cooling.

Indeed, using the temperature investigations of crystal–optical characteristics in a low-temperature region, we established the presence of phase transformations in both states (A and B) of $K_2WO_2F_4 \cdot H_2O$. Crystals A stored in humid atmosphere undergo the

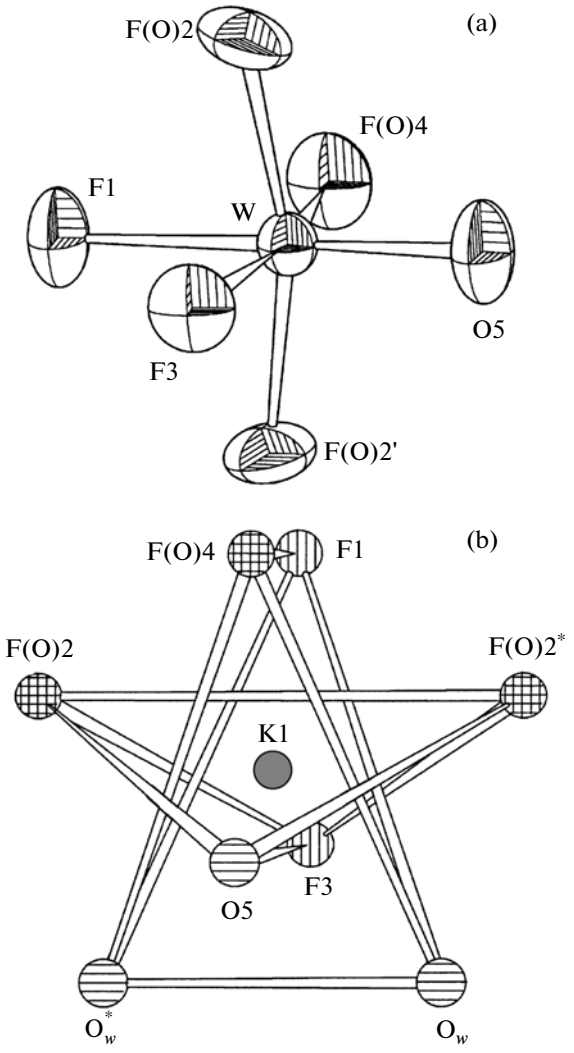

Fig. 4. Main structural polyhedra of the $K_2WO_2F_4 \cdot H_2O$ crystal. (a) The structure of the (WO_2F_4) oxyfluoride complex and (b) nearest surrounding of the K1 atom. O_w is the oxygen of crystallization water. Asterisks and dashes are introduced for visual distinction of symmetrically identical atoms.

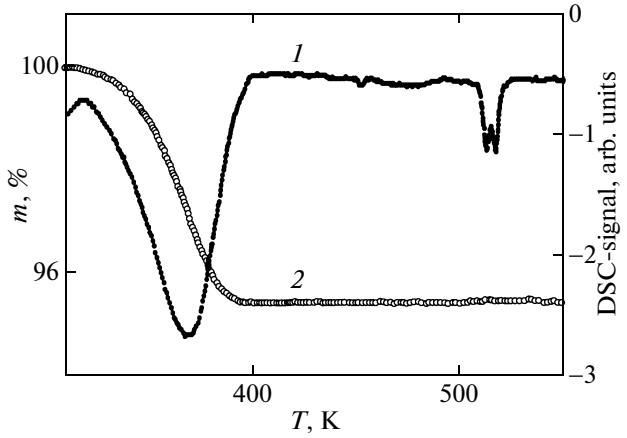

Fig. 5. Results of investigations of the $K_2WO_2F_4 \cdot H_2O$ crystal by synchronous thermal analysis. (*1*) DSC data and (*2*) TG data.

reversible phase transition $G_3 \longleftrightarrow G_2$ near the melting point of ice, which is accompanied by twinning, appearance of the shift deformation x_6, and rotation of the optical indicatrix for the angle $\varphi_c \approx \pm 50°C$. As a result of this transition, the symmetry elements of the group $C2/m$ such as the second-order axis and mirror plane are lost. We select the symmetry group of the low-temperature phase G_3 is $P\bar{1}$. We assume that this second-order transition with the exponent $\beta = 0.36$ depending on $\eta(T_{03} - T)$ is the proper ferroelastic transition $\delta n_c(T) \sim \varphi(T) \sim \eta(T) \sim x_6(T)$, where δn_c is the anomalous part of birefringence, η is the transition parameter, and x_6 is the component of the shear deformation appeared as a result of the phase transition at T_{03}.

No low-temperature ferroelastic phase transition was observed for crystal B stored for a long time at relative humidity lower than 20%. After the phase transition at $T'_{03} = 263$ K ($G_3 \longleftrightarrow G_2$), the symmetry class remains invariable. The crystal system remains monoclinic, but the appearance of twins with shapeless boundaries in the G_3 phase allows us to assume the loss of the second-order axis of the symmetry group $C2/m$. This can be the result of ordering the structural water in one of two sites relative to the second-order axis.

According to observations in the polarized light, the $K_2WO_2F_4 \cdot H_2O$ crystal (samples A and B) above T_{02} (phase G_1) becomes optically uniaxial (tetragonal). The first-order transition between the phases $G_2 \longrightarrow G_1$ occurs in a temperature range $T_{02} \approx 350$–380 K and above (this depends on the experimental rate), which is accompanied by cracking of the crystal. However, this transition has distinctive features for crystals A and B. In sample A, the phase transition at T_{02} is characterized by a prolonged relaxation time and can be reversible at the first stage. In this case, the sample during cooling undergoes the ferroelastic phase transition at T_{03}, while the transition into phase G_1 in crystals B is irreversible.

To acquire the additional information on high-temperature transitions, we used the method of synchronous thermal analysis (STA), which combines the gravimetric (TG) and calorimetric (DSC) methods. The measurements were performed using a NETZCH STA 449 Jupiter device in the temperature range 310–560 K with a rate of 2 K/min (Fig. 5). Two endothermic DSC peaks corresponding to temperatures T_{02} and T_{01} are observed in curve *1*. The weight loss (TG) (curve *2*) occurs only near T_{02} and constitutes $\delta m = 4.6 \pm 0.1\%$, which corresponds to the weight of struc-

tural water. Repeated recording shows no anomalies in the TG and DSC curves at T_{02}. However, crystallization water restores for a day, and anomalies at T_{02} become observable again. The endothermic peak at $T_{01} \approx 510$ K is clearly seen in the DSC curve, although the substance weight is invariable. The X-ray investigations showed that $K_2WO_2F_4$ gradually decomposes in this temperature region. Optical experiments showed the complete loss of transparence of the samples.

6. CONCLUSIONS

Performed investigations showed that depending on the storage conditions, the $K_2WO_2F_4 \cdot H_2O$ crystal has two states. These are the crystals stored at relative humidity above 20% (sample A) and at relative humidity lower than 20% (sample B). Room-temperature X-ray investigations of the $K_2WO_2F_4 \cdot H_2O$ single crystals showed the complete coincidence of the structure and symmetry ($C2/m$) of this substance in states A and B.

The $K_2WO_2F_4 \cdot H_2O$ crystal in both states undergoes the sequence of reversible and irreversible phase transformations $G_3 \longleftrightarrow G_2 \longrightarrow G_1 \longrightarrow G_0$ in the temperature range 100–600 K. The irreversible first-order transition $G_2 \longrightarrow G_1$ between the monoclinic and tetragonal phases occurs in the temperature range $T_{02} \approx$ 350–380 K. It is accompanied by cracking of the crystal and the loss of crystallization water. In the G_1 phase, the $K_2WO_2F_4$ crystal has tetragonal symmetry $P4/mmm$ [15], which is retained during cooling to 100 K. Structural water is easily absorbed from atmosphere for a day. The $G_1 \longrightarrow G_0$ transition is a high-temperature decomposition of the substance. The main distinction between crystals A and B occurs in a low-temperature region. During the second-order phase transition $G_3 \longleftrightarrow G_2$ in crystal A, the symmetry changes as $P\bar{1} \longleftrightarrow C2/m$. This proper ferroelastic transition is accompanied by the appearance of the shear deformation x_6. The crystal system of the substance in the crystal B does not vary during the second-order phase transition $G_3 \longleftrightarrow G_2$: $m \longleftrightarrow C2/m$. The difference between crystals A and B is explained by the possible presence of free water in interlayer spaces of samples A, which can compensate the loss of the part of crystallization water transforming the transition at T_{02} (at the initial stage) from irreversible into the reversible. Freezing of this water at $T \approx 270$ K causes the ferroelastic transition at T_{03}. The weight of this water is small and constitutes no more than 0.1% of the total weight of the substance. It is possible that the existing spread of the values $T_{03} = 270$–290 K in different samples is explained by the difference in amounts of free water in them. It is established that at elevated air humidity, water penetrates into the interlayer space for several hours transforming crystal B into crystal A.

Thus, the studied crystal, similarly to cleaved aluminosilicates (montmorillonite, bentonite, etc.) is very sensitive to the vapor concentration in air. However, when penetrating into the interlayer spacings, free water changes the properties of the substance with the crystal structure being invariable.

ACKNOWLEDGMENTS

We thank A.V. Cherepakhin for STA investigations.

This work was supported by the Presidential Grant of the Russian Federation NSh-4645.2010.2, by the Russian Foundation for Basic Research, project no. 09-02-00062, and by the Integration Project of the Siberian Branch of the Russian Academy of Sciences no. 101.

REFERENCES

1. A. M. Strivastava and J. F. Ackerman, J. Solid State Chem. **98**, 144 (1992).
2. V. M. Sergienko, M. A. Porai-Koshits, and T. S. Khodashova, J. Struct. Chem. **13** (3), 431 (1972).
3. M. Vlasse, J. M. Moutou, M. Cervera-Marsal, J. P. Chaminade, and P. Hagenmuller, Rev. Chim. Miner. **19**, 58 (1982).
4. A. A. Udovenco and N. M. Laptash, Acta Crystallogr., Sect B: Struct. Sci. **64**, 645 (2008).
5. G. Z. Pinsker and V. G. Kuznetsov, Sov. Phys. Crystallogr. **13** (1), 56 (1968).
6. G. Z. Pinsker, Sov. Phys. Crystallogr. **11** (5), 634 (1966).
7. K. R. Heier, A. J. Norquist, P. S. Halasyamani, A. Duarte, C. L. Stern, and K. R. Poeppelmeier, Inorg. Chem. **38**, 762 (1999).
8. A. A. Udovenco and N. M. Laptash, Acta Crystallogr., Sect. B: Struct. Sci. **64**, 527 (2008).
9. S. V. Mel'nikova, V. D. Fokina, and N. M. Laptash, Phys. Solid State **48** (1), 117 (2006).
10. S. V. Mel'nikova and N. M. Laptash, Phys. Solid State **50** (3), 511 (2008).
11. V. D. Fokina, E. V. Bogdanov, M. V. Gorev, M. S. Molokeev, E. I. Pogorel'tsev, I. N. Flerov, and N. M. Laptash, Phys. Solid State **52** (4), 781 (2010).
12. D. Grandjean and R. Weiss, Bull. Soc. Chim. Fr., No. 8, 3040 (1967).
13. D. Grangjean and R. Weiss, Bull. Soc. Chim. Fr., No. 8, 3049 (1967).
14. D. Grangjean and R. Weiss, Bull. Soc. Chim. Fr., No. 8, 3054 (1967).
15. Z. H. Jie, A. Garcia, F. Guillen, J.-P. Chaminade, and C. Fouassier, Eur. J. Solid State Inorg. Chem. **30**, 773 (1993).
16. G. M. Sheldrick, Acta Crystallogr., Sect. A: Found. Crystallogr. **64**, 112 (2008).